Astron. Nachr. / AN **335**, No. 2, 150 – 160 (2014) / **DOI** 10.1002/asna.201211953

Brightness fluctuations of the Sun and p-mode oscillations: The inverse problem and nonadiabatic waves in the photosphere

A. Prokhorov[1,⋆], **Y.D. Zhugzhda**[1,2], and **S. Berdyugina**[1]

[1] Kiepenheuer-Institut für Sonnenphysik Freiburg im Breisgau, Schöneckstr. 6, D-79104 Freiburg, Germany
[2] Pushkov Institute of Terrestrial Magnetism, Ionosphere and Radio Wave Propagation of the Russian Academy of Sciences, Russian Federation, 142190, Troitsk, Moscow reg.

Received 2013 Jul 21, accepted 2013 Aug 8
Published online 2014 Feb 3

Key words Sun: helioseismology – Sun: interior – Sun: oscillations – radiative transfer – waves

Using photometric observations of the Sun as a star (DIFOS, SoHO) we were able to solve the inverse heloiseismic problem and determine the global time-dependent relative temperature fluctuations as functions of the geometric height. This was done under the adiabatic assumption. A mathematical tool was developed to solve the inverse problem, which is ill-posed. The calculations were done using the numerical software Matlab 7. The adiabatic solution shows signs of temperature waves in the lower photosphere, which agrees with calculations done by Rodríguez Hidalgo et al. (2001) and Stodilka (2011).

1 Introduction

Helioseismology is a large step forward in the precision of the internal structural model of the Sun. Asteroseismology aims to obtain similar improvements for different types of stars by means of their oscillations. Stellar oscillations are the only diagnostic known that allows us to improve the stellar structure and evolution models by at least one order of magnitude. Asteroseismology is growing research field because the observations of thousands of stars become available by the presently operational CoRoT and *Kepler* missions, which have brought results of unprecedented precision on the pulsations of stars of all types. Thus, the observations of brightness fluctuations of stars by CoRoT and *Kepler* missions and other future space missions are the main source of data on star oscillations. Consequently, the theory of brightness oscillations of stars is needed to explore space photometric observation of stars. As usual, the exploration of the brightness oscillations of the Sun is used as a basement for the understanding of the brightness fluctuations of stars.

The brightness fluctuations of stars are considered by some authors as a result of changes in the effective temperature of a star ((Ballot et al. 2011)). This assumption can be used only as a very rough approximation. In fact, brightness oscillations of stars are defined by the visibility of the modes of star oscillations. The visibility equals the integral of the product of spherical harmonic and limb darkening function over the stellar disc. The center-limb darkening function for p-modes is defined as a function of the amplitude of brightness oscillation on radial distance. This limb darkening function must not be confused with limb darkening functions of the quiet Sun and stars. In order to calculate the visibility function, the eigenfunction of p-mode is needed because fluctuation of radiative flux in photosphere depends on disturbances of temperature and density. The temperature fluctuations affect the Planck function while opacity and, consequently, optical depth are affected by both temperature and density. The visibility functions were explored by Toutain & Gouttebroze (1993), Staude et al. (1994), Zhugzhda et al. (1996), and Fontenla et al. (2006). Toutain & Gouttebroze (1993) used a numerical code for the calculations of eigenfunctions while Staude et al. (1994), Zhugzhda et al. (1996), and Fontenla et al. (2006) used a crude approximation for the qualitative analysis of the properties of visibility functions. In all cases, a non-gray approximation has been used since a gray approximation leads to wrong results.

An alternative approach for the treatment of the problem is to use data of multi-color photometric observations of the brightness oscillations of the Sun with DIFOS and SoHO (Lebedev et al. 1995; Hasler et al. 1997). These observations provide data for a solution of the inverse problem which defines the dependence of the temperature and density fluctuations in the photosphere. The first steps on this way were done by Staude et al. (1994), Zhugzhda & Lebedev (2009), and Stodilka (2011). Besides, Rodríguez Hidalgo et al. (2001) used ground-based spectral observations to solve the inverse problem for local oscillation in the solar atmosphere. The inverse problem belongs to an ill-posed problems. So far, a Tichonov regularization (Stodilka 2011), a Monte Carlo algorithm (Rodríguez Hidalgo et al. 2001), and a polynomial approximation (Zhugzhda & Lebedev 2009) have been used to solve the inverse problem.

⋆ Corresponding author: anton@kis.uni-freiburg.de

The problem of the brightness fluctuations of pulsating stars has to be discussed in frame of the theory of nonadiabatic waves. On the first sight, the theory of nonadabatic waves is well developed (see Mihalas & Mihalas 1984; Zhugzhda 1983; Zhugzhda et al. 1993; Staude et al. 1994, and references therein). But there is one shortcoming in all these explorations – the radiative flux through the atmosphere is not taken into account. This leads to difficulties in the application of the theory to the analysis of brightness oscillation, because the photosphere is formed by the radiative flux of the star.

This paper is structured as follows: First we formulate the problem of finding the temperature and density as an inverse ill-posed problem and discuss possible mathematical problems (Sect. 2). Then, we outline the observational data to be used to solve the inverse problem (Sect. 3). Subsequently, we show in Sect. 4 the results for the partial derivatives of the opacity, which are needed for further calculations. In Sect. 5 we present our subjective theory for solving the ill-posed problem using only general mathematical assumptions. In order to test the applicability of our theory, we solved the inverse problem for the adiabatic case, and the results are shown in Sect. 6. Finally, the results are discussed in the frame of the theory of nonadiabatic waves.

2 Formulation of the problem

The total flux at a chosen frequency can be written in the well-known form, used by Mihalas & Mihalas (1984), Sect. 6.5[1]:

$$F_\nu = \int_{-1}^{1} \left(\int_0^\infty B_\nu(T(\tau_\nu))\, \mathrm{e}^{-\tau_\nu/\mu}\, \mathrm{d}\tau_\nu \right) \mathrm{d}\mu\,, \tag{1}$$

where μ is the angle to the normal of the Sun's surface, $B_\nu(T)$ the source function, which in the LTE case is equal to the Planck function, T is the temperature, and τ_ν is the optical depth scale, which is related to the opacity $\kappa_\nu(\rho, T)$ and geometrical height scale z as follows:

$$\mathrm{d}\tau_\nu = -\kappa_\nu\, \mathrm{d}z, \tag{2}$$

$$\tau_\nu = -\int_\infty^{z(\tau_\nu)} \kappa_\nu\, \mathrm{d}z. \tag{3}$$

The opacity is commonly defined as a function of density and temperature, which are in turn functions of either the geometrical height or optical depth. Consequently, one has two functions: $\kappa_\nu(z)$ and $\kappa_\nu(\tau_\nu)$. Since we assume the relation (3) to be objective, we make no difference between these two functions.

It is important to mention that, in case of observations of the Sun as a star, all defined quantities are averaged over the surface and depend additionally on time. We now build the first variation of the flux with respect to the time, assuming all functions to be continuous and differentiable. This assumption is important if one wants to calculate the variation of an integral using the variation of the integrand and which is common among physicists. Hence,

$$\delta F_\nu = \int_{-1}^{1} \left(\int_0^\infty \delta \left\{ B_\nu(T(\tau_\nu))\, \mathrm{e}^{-\tau_\nu/\mu}\, \mathrm{d}\tau_\nu \right\} \right) \mathrm{d}\mu\,. \tag{4}$$

The variation of the integrand can be calculated as follows:

$$\delta \left\{ B_\nu\, \mathrm{e}^{-\tau_\nu/\mu}\, \mathrm{d}\tau_\nu \right\} = \left(\frac{\mathrm{d}B_\nu}{\mathrm{d}T}\, \delta T\, \mathrm{d}\tau_\nu + B_\nu \delta\, \mathrm{d}\tau_\nu \right) \mathrm{e}^{-\tau_\nu/\mu} - \frac{B_\nu}{\mu} \delta\tau_\nu\, \mathrm{d}\tau_\nu\, \mathrm{e}^{-\tau_\nu/\mu}. \tag{5}$$

The total variation of the integrand combines variations of the temperature and the following variations of the optical depth scale. The latter depends indirectly on the temperature by means of the opacity. To insert it in our calculations, we combined Eqs. (2) and (3) with

$$\delta \mathrm{d}\tau_\nu = -\delta\kappa_\nu\, \mathrm{d}z = \frac{\delta\kappa_\nu}{\kappa_\nu}\, \mathrm{d}\tau_\nu \tag{6}$$

and

$$\delta\tau_\nu = -\int_\infty^{z(\tau_\nu)} \delta\kappa_\nu\, \mathrm{d}z = \int_0^{\tau_\nu} \frac{\delta\kappa_\nu}{\kappa_\nu}\, \mathrm{d}\tau'_\nu. \tag{7}$$

The total flux variation becomes

$$\delta F_\nu = \int_0^\infty \left(\frac{\mathrm{d}B_\nu}{\mathrm{d}T} \delta T + B_\nu \frac{\delta\kappa_\nu}{\kappa_\nu} \right) E_2(\tau_\nu)\, \mathrm{d}\tau_\nu - \int_0^\infty B_\nu \left(\int_0^{\tau_\nu} \frac{\delta\kappa_\nu}{\kappa_\nu} \mathrm{d}\tau'_\nu \right) E_1(\tau_\nu)\, \mathrm{d}\tau_\nu, \tag{8}$$

where

$$E_n(x) = \int_1^\infty \frac{\mathrm{e}^{-xt}\mathrm{d}t}{t^n} \tag{9}$$

is called the exponential integral.

A similar equation for the intensity variation, i.e. with no integration over the angle, was derived by Staude et al. (1994). However, the third term significantly differs from our result. This discrepancy can be overcome by integrating the third term by parts and will be skipped. Another derivation of the relative flux oscillations can be found in Toutain & Gouttebroze (1993).

Skipping the angle integration in Eq. (8) defines the absolute flux oscillation at a given ν for a given angle μ – the (spectral) darkening function (Zhugzhda et al. 1996). In order to complete the relation (8), we introduce

$$\frac{\delta\kappa_\nu(\rho, T)}{\kappa_\nu} = \left(\frac{\partial \ln\, \kappa_\nu}{\partial \ln\, \rho} \right) \frac{\delta\rho}{\rho} + \left(\frac{\partial \ln\, \kappa_\nu}{\partial \ln\, T} \right) \frac{\delta T}{T} \tag{10}$$

and use the logarithmic representation since it has the advantage of being dimensionless.

Equations (8) and (10) define the flux variation in time in LTE in a plane parallel atmosphere as a function of density and temperature perturbations. The visible (relative) flux oscillations $\delta F_\nu / F_\nu$ at a specific frequency ν can be observed, so that in principle it is possible to solve the introduced integral equation for $\delta\rho/\rho$ and $\delta T/T$. We chose these dimensionless combinations due to numerical advantages.

[1] See also Mihalas (1970), Sect. 1.4.

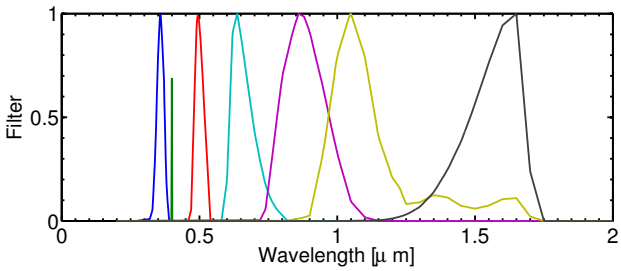

Fig. 1 Transmission functions T_f for the DIFOS experiment (Link). The filter at 400 nm corresponds to the SPM instrument installed onboard the SOHO observatory.

Table 1 Consolidation of the observational results using the DIFOS and SPM photometer.

Wavelength [nm]	Amplitude [10^{-6}]	Phase [grad]
357	4.25	–16
402 (SPM)	4.36	18
494	3.05	16
637	2.25	10
860	1.65	0
1100	1.44	0
1650	0.75	30

The problem of solving Eqs. (8) and (10) for $\delta\rho/\rho$ and $\delta T/T$ is called inverse and is ill-posed (Press et al. 2007, Sect. 19.0). In order to illustrate this, we briefly mention that an integral is not a unique functional of its integrand, since to a given area it is possible to find an infinite number of different curves covering the same area. From this point of view, the solution of an ill-posed problem is always subjective. We will present our solution in Sect. 5.

3 Observational data

The observed flux oscillation is well represented by

$$\frac{(\delta F_\nu)_{\rm obs}}{(F_\nu)_{\rm obs}} = A_\nu \cos(\omega t + \Delta\varphi_\nu). \quad (11)$$

The observational data are represented by the measured amplitude A_ν of the relative flux fluctuations and the phase difference $\Delta\varphi_\nu$, which is measured with respect to $\delta F_\nu/F_\nu$ at 860 nm. The observation was performed by means of the DIFOS photometer onboard the CORONAS-F satellite (Zhugzhda & Lebedev 2009) and is shown in Table 1. An additional observation, performed by means of the SPM photometer at 402 nm (Wehrli et al. 1997) was added to our data.

The DIFOS photometer observed the Sun as a star at 6 different channels. The frequency filters T_f of photometers are rather wide (Fig.1). The bandwidth of the violet channel was $\approx$50 nm, and $\approx$200 nm for the near infrared regions. In order to calculate the response of photometers, an integration over the frequency is needed:

$$(\delta F_\nu)_{\rm obs} = \int_0^\infty T_f\, \delta F_\nu \, {\rm d}\nu, \quad (12)$$

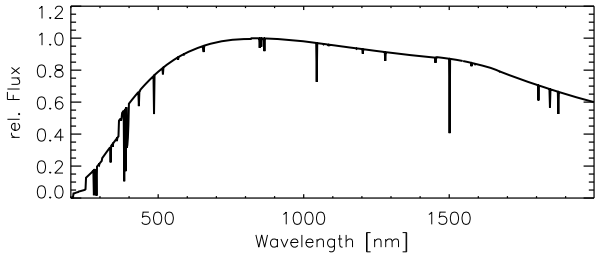

Fig. 2 Synthetic flux normalized to the maximum value at 800 nm. Solution of the 1D radiative transfer in the FAL-C model atmosphere (Fontenla et al. 2006). Some strong lines were included in the calculations; wavelength range: [200 nm, 2000 nm].

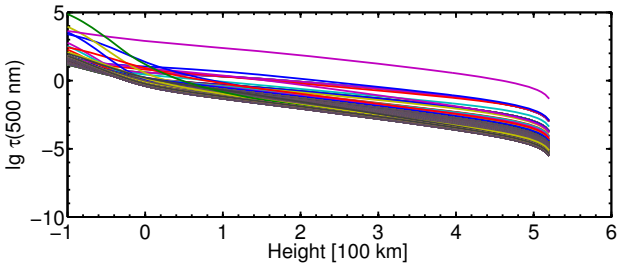

Fig. 3 $\lg \tau_{500}$ vs. geometrical height for wavelengths from 0.2 μm to 2 μm.

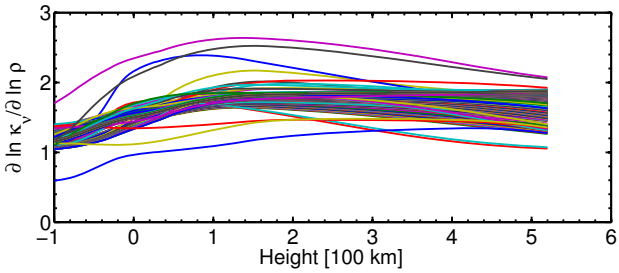

Fig. 4 $(\partial \ln \kappa_\nu/\partial\, ln\, \rho)$ vs. geometrical height for wavelengths from 0.2 μm to 2 μm.

$$(F_\nu)_{\rm obs} = \int_0^\infty T_f F_\nu \, {\rm d}\nu. \quad (13)$$

Measurements of the amplitude and phases of brightness oscillations provide real and imaginary parts of $(\delta F_\nu)_{\rm obs}$. This implies that the solution of the inverse problem has to be performed separately for both parts.

4 Calculation of the partial derivatives

The variation of the opacity (Eq. 10) is the crucial point in our approach, since it depends on partial derivatives that are a-priori unknown. In order to obtain the derivatives, in general one has to solve a complete set of magnetohydrodynamic equations with an appropriate equation of state for the opacity. This task is impossible to solve analytically. Nutto et al. (2008) dealt with the same problem and used the RH-Code written by H. Uitenbroek (Uitenbroek 2001) to solve the radiative transfer equation in the 1D (Sun as a star) model atmosphere FAL-C (Fontenla et al. 2006). The

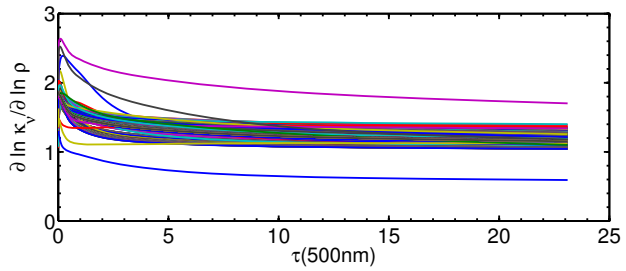

Fig. 5 $(\partial \ln \kappa_\nu / \partial \ln \rho)$ vs. τ_{500} for wavelengths from 0.2 μm to 2μm.

Table 2 Atoms and molecules, considered for opacity calculations.

Atoms	H, C, O, Si, Al, Ca
Molecules	H_2, H_2^+, C_2, N_2, O_2, CH
Atoms	Fe, He, Mg, N, Na, S, Ti
Molecules	CO, CN, NH, NO, OH, H_2O, TiO

code is based on the Rybicky and Hummer Multi-Level Approximate Lambda Iteration formalism (Rybicki & Hummer 1992); it solves multidimensional radiative transfer using the short-characteristics method (Kunasz & Auer 1988) and is able to calculate the opacities in a given model atmosphere using a given set of atoms and molecules together with specified absorption lines in LTE and non-LTE. Certainly, these calculations are not necessarily complete from the physical point of view, since they do not implement, for example, the effects of the magnetic field on the molecular lines. We believe however, that the strength of these effects is negligible if one considers the Sun as a star.

For our further calculations we repeated the analysis done by Nutto et al. (2008) for the same model atmosphere. Atoms and molecules considered for the opacity calculations are listed in Table 2. We want to stress the presence of the TiO molecule in our calculations, which was not considered by Nutto et al. (2008). We now introduce the dimensionless visibility function

$$V_\nu(\delta T) = \frac{\delta F_\nu}{F_\nu}, \tag{14}$$

pointing out that the analysis done by Nutto et al. (2008) assumed $(\delta T/T) \approx \text{const}$. This will be ignored in the following.

In order to calculate the derivatives, we used the original FAL-C model atmosphere and introduced small temperature (1 K) and density (10^{-6} g cm^{-3}) perturbations corresponding to $<0.1\,\%$ of the average values. The radiative transfer was then solved for both (original and modified) atmospheres in 1D under the LTE assumption. The synthesized flux is shown in Fig. 2 and is normalized to its maximal value. Some strong atomic lines, that are shown in the figure, were included in the calculations. The optical depth scale as a monotonic function of geometrical height is shown in Fig. 3. The geometrical height scale has its null-point at $\tau_{500} = 1$. The optical depth ranges from 10^5 to 10^{-5}, so that the emergent intensity at all wavelengths arises from layers at height 0 ± 40 km.

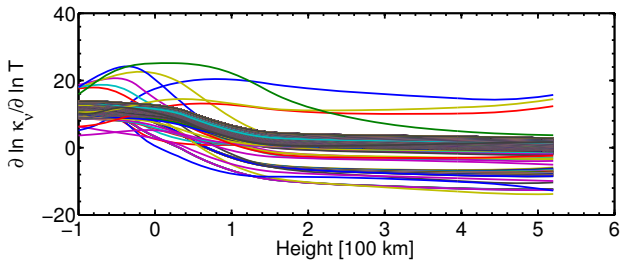

Fig. 6 $(\partial \ln \kappa_\nu / \partial \ln T)$ vs. geometrical height for wavelengths from 0.2 μm to 2 μm.

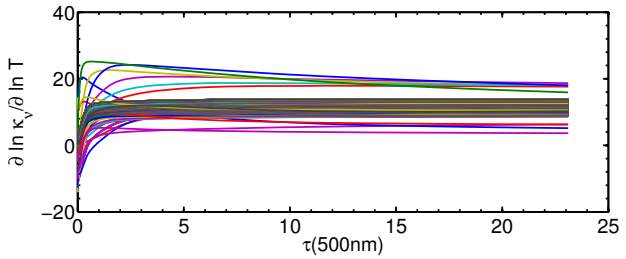

Fig. 7 $(\partial \ln \kappa_\nu / \partial \ln T)$ vs. τ_{500} for wavelengths from 0.2 μm to 2 μm.

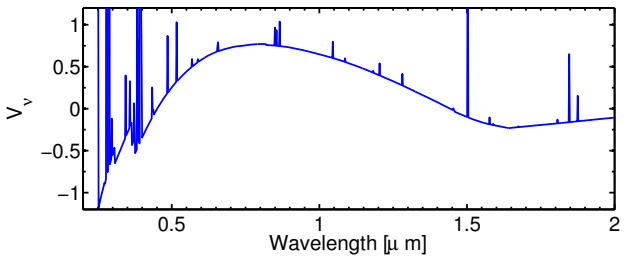

Fig. 8 Synthetic visibility function for the FAL-C model atmosphere.

Using the opacities from both radiative transfer solutions, we calculated the derivatives, which are shown in Figs. 4–7. The choice of the X-axis affects the behavior of the derivatives, which are monotonic functions of τ_{500} but become non-monotonic in the rest of the plots. The average values of the derivatives with respect to the geometrical height are[2]

$$\left(\frac{\partial \ln \kappa}{\partial \ln T}\right) \approx 3.7 \pm 2 \tag{15}$$

$$\left(\frac{\partial \ln \kappa}{\partial \ln \rho}\right) \approx 1.7 \pm 0.1. \tag{16}$$

The result is in general agreement with Nutto et al. (2008) and shows that opacity depends on the temperature rather than on the density. The appropriate derivative is also more sensitive to strong atomic lines.

Using the introduced derivatives we calculated the visibility function $V_\nu(\delta T = 1)$ by means of Eq. (8) with

[2] Format is mean ± standard deviation.

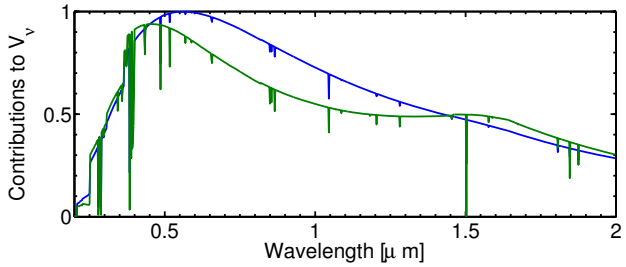

Fig. 9 Different contributions (normalized) $\partial B_\nu/\partial \ln T$ (blue) and $\partial \ln \kappa_\nu/\partial T + \partial \ln \kappa_\nu/\partial \rho$ (green) to the visibility function.

$\delta T = 1\,\mathrm{K}$ and the adiabatic assumption $\delta\rho = \rho\frac{1}{5/3-1}\frac{\delta T}{T}$ as was done by Zhugzhda & Lebedev (2009). The resulting curve (Fig. 8) shows a non-monotonic behavior with respect to the wavelength. This agrees well with the result of Zhugzhda & Lebedev (2009). What is particularly interesting are spectral regions with negative values (near ultraviolet and infrared), where any positive temperature perturbation would result in negative flux variations. Since the first and second terms in Eq. (8) are strictly positive, the only reason for the mentioned negative connection between δT and δF_ν is the third term in Eq. (8) which goes with the negative sign in the integral.

In the following, we separated the first term (flux fluctuation due to the Planck function) from the others (flux fluctuations due to opacity changes), wrote Eq. (8) as follows:

$$\delta F_\nu = \int_0^\infty \left(\frac{\mathrm{d}B_\nu}{\mathrm{d}T}\right)\delta T \mathrm{d}\tau_\nu + \int_0^\infty \ldots\,, \qquad (17)$$

and studied the behavior of the two parts separately from each other (Fig. 9). The figure shows that in the mentioned spectral regions, <500 nm and >1400 nm, the contribution of the second term (opacity) is of the same order and even higher than the contribution originating from the Planck function. This means, that a sign change in the near ultraviolet and infrared happens not directly due to the temperature, but due to the opacity fluctuations.

This also shows, that even such a simple model can provide results which were not directly expected.

5 Solution of the inverse problem

In order to solve Eq. (8) for the unknown $\delta T/T$ and $\delta\rho/\rho$ for a given set of (spatial) points $z \in \{z_1 > z_2 > \ldots > z_N\}$, additional restrictions on the shape of the solution are necessary. In order to find $\delta T/T$ and $\delta\rho/\rho$, Eq. (8) has to be written as a matrix equation, solvable by means of modern mathematical software, e.g. Matlab. There are several possibilities to do that.

But first we simplify the approach by choosing the adiabatic approximation, i.e.

$$\delta\rho = \rho\frac{1}{\Gamma-1}\frac{\delta T}{T}, \qquad (18)$$

where $\Gamma = 5/3$ is the adiabatic exponent. In this case the number of unknowns reduces by a factor of 2. The adiabatic approximation assumes that the oscillations do not differ essentially from pure adiabatic ones, which is why the latter is referred to as quasi-adiabatic approximation. Toutain & Gouttebroze (1993) explored the effect of different approximations on visibility function, namely, adiabatic, nonadiabatic, and isothermal approximations. The comparison with observations led authors to the conclusion that the adiabatic approximation provides the best agreement with observations. This conclusion is in contradiction with the relaxation times of temperature disturbances in the solar photosphere which lie between two extremes: adiabatic and isothermal cases. Thus, the nonadiabatic approximation appears to be more reasonable for the solar photosphere. But the relaxation times are defined by the effect of temperature fluctuations on blackbody emission. Brightness fluctuations due to opacity fluctuations are out of phase with blackbody emission. This leads to an increase in effective relaxation times in the photosphere. The blackbody and opacity effects are of the same order as shown in Fig. 9. Consequently, the adiabatic approximation is not as bad as it looks on the first sight.

Besides, Toutain & Gouttebroze (1993) argue that the blackbody approximation has to be used for the visibility function calculation. The blackbody approximation ignores the effect of opacity fluctuations on the visibility function. The qualitative analysis of Nutto et al. (2008) shows that opacity fluctuations affect the visibility function of solar p-modes. The numerical calculations of Toutain & Gouttebroze (1993) show that the visibility function is sensitive to opacity fluctuations. Nevertheless, the analysis by Toutain & Gouttebroze (1993) leads to the conclusion that the blackbody approximation provides better agreement with observations. It is important to mention that the exploration of Toutain & Gouttebroze (1993) was based on data of the IPHIR experiment which provides the first observations of the brightness of the Sun from space. This experiment was performed before the SoHO and CORONAS experiments. However, the authors did not take into account the phase shift between the different spectral channels. The exploration of Toutain & Gouttebroze (1993) was not repeated with new data in spite of the contradiction with the application of adiabatic and blackbody approximations. Nevertheless, the authors conclusions on the preference of adiabatic and blackbody approximations for the treatment of the visibility function are used in many cases. We do not think that there are any reasons to use the blackbody approximation.

The simplest way to solve the inverse problem discussed by Zhugzhda & Lebedev (2009) is to use the adiabatic case and to express the remaining unknown $\delta T/T$ as a polynomial in z: $\sum_{i=0}^{L} A_i z^i$. The number of the unknown parameters in Eq. (10) is halved due to the adiabatic approximation, and the flux perturbations depend only on temperature,

$$\delta F_\nu = \int_{z_1}^{z_N} \frac{\delta T(z)}{T} K(z,\nu)\,\mathrm{d}z, \qquad (19)$$

with known kernel $K(z,\nu)$. Thanks to the polynomial shape of $\delta T/T$, an insertion into Eq. (19) would immediately re-

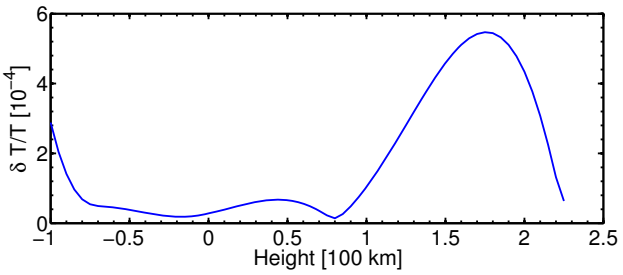

Fig. 10 Absolute value of the solution of the inverse problem (19) using observational data from Table 1 and ignoring the integration (12). Polynomial assumption $\delta T/T = \sum_{i=0}^{6} A_i z^i$.

sult in a simple matrix equation, exactly solvable for the coefficients A_i, if the order of the polynomial L is equal to the number of given flux fluctuations increased by one (Fig. 10).

The advantage of this solution is the fact that the unknown coefficients are constants and can be written outside the integrals. The integrals itself can be calculated numerically with high precision. The main problem, however, is obviously the order of the polynomial which can be high. Such a polynomial would commonly tend to oscillations of an unphysically high amplitude (3 K in Fig. 10) and even diverge in higher layers (low τ).[3]

In order to overcome this difficulty while maintaining the polynomial shape of the solution, the functions $\delta T/T$ and $\delta\rho/\rho$ can be expressed as splines, i.e. (different) polynomials of some small order (say, 1–3) with separate, in general linearly independent, coefficients in each interval $[z_{i-1}, z_i]$:

$$\frac{\delta T}{T} = \sum_{j=0}^{L} A_{ij}(z - z_i)^j, \tag{20}$$

$$\frac{\delta \rho}{\rho} = \sum_{j=0}^{L} B_{ij}(z - z_i)^j. \tag{21}$$

Since there are in general $N-1$ intervals, there are $(N-1)(L+1)$ unknown coefficients for each function, which would require at least the same (large) number of given flux oscillations at different wavelengths for the solution to be exact, which is technically not possible. Besides this purely technical problem, the assumption of a solution jumping from interval to interval is unphysical as well. In order to deal with this, we defined the following restrictions to the solutions:

- polynomial,
- continuous,
- $L-1$ times differentiable.

The continuity conditions for $\delta T/T$, $\delta\rho/\rho$ and their $L-1$ derivatives reduce the number of the unknowns to $N+L$ times 2, for there are $L+1$ unknowns in the first, and additionally one in each other interval for each function.

The further reduction of Eq. (19) to a matrix equation using spline representations is similar to the method described in Kurucz (1969), originally applied to radiative transfer problems. Together with Eq. (21), Eq. (8) becomes

$$\delta F_\nu = \sum_{i=1}^{N-1} \sum_{j=0}^{L} A_{ij} C_{ij\nu} + B_{ij} D_{ij\nu} = \operatorname{span}(A^T C_\nu + B^T D_\nu), \tag{22}$$

with

$$C_{ij\nu} = -\int_{z_i}^{z_{i+1}} (z - z_i)^j \times \left\{ \frac{\mathrm{d}B_\nu}{\mathrm{d}\ln T} + B_\nu \frac{\partial \ln \kappa_\nu}{\partial \ln T} \right\} E_2 \kappa_\nu \,\mathrm{d}z - \int_{z_i}^{z_{i+1}} B_\nu E_1 \kappa_\nu \int_{z_1}^{z} (z' - z_i)^j \frac{\partial \ln \kappa_\nu}{\partial \ln T} \kappa_\nu \,\mathrm{d}z' \mathrm{d}z, \tag{23}$$

$$D_{ij\nu} = -\int_{z_i}^{z_{i+1}} (z - z_i)^j B_\nu E_2 \frac{\partial \ln \kappa_\nu}{\partial \ln \rho} \kappa_\nu - \int_{z_i}^{z_{i+1}} B_\nu E_1 \kappa_\nu \int_{z_1}^{z} (z' - z_i)^j \frac{\partial \ln \kappa_\nu}{\partial \ln \rho} \kappa_\nu \,\mathrm{d}z' \mathrm{d}z. \tag{24}$$

The matrices $C_{ij\nu}$ and $D_{ij\nu}$[4] are known, since the integrals (23) and (24) can be numerically calculated and the solution of the inverse problem is now reduced to the solution of Eq. (22) for A_{ij} and B_{ij}. Due to the continuity conditions, most of A_{ij} and B_{ij} are linear dependent and can be consolidated (Eq. 22) by defining the vectors x, consisting of the $2(N+L)$ linear independent unknowns

$$\delta F_\nu = \tilde{C} x^T. \tag{25}$$

The matrix $\tilde{C} \in M(2(N+L), \#\nu)$ arises as a result of the consolidation and consists of $2(N+L)$ rows and $\#\nu$ columns.

Even after the described mathematical and physical simplifications the matrix equation (25) does not guarantee an exact and physically acceptable solution. From the theoretical point of view, the matrices $C_{ij\nu}$ and $D_{ij\nu}$ are ill-conditioned in terms of the ratio between the maximal and minimal eigenvalues (it achieves values $>10^{20}$). The reason for this lie in the construction of (23) and (24) and, more precisely, in the choice of the grid z_i. If the grid is equidistant, most $C_{ij\nu}$ and $D_{ij\nu}$ calculated at higher altitudes are due to extremely small values of the integrand, almost equal within the numerical accuracy. The same behavior could be determined also in deeper layers (high τ), where high values of the source function are dumped by the extremely small values of the exponential integral. As a result, the rows of $C_{ij\nu}$ and $D_{ij\nu}$ are almost linearly dependent and the solution of (25) is perturbed by numerical uncertainties.

The mentioned feature can be fixed by using an adapted grid defined in such way, that the integrals (23) and (24)

[3] Figure 10 shows only a small part of the solution near to convection. The behavior of the solution in the higher layers is completely unphysical since it reaches values of the order 10^3 K.

[4] The third index describes the wavelength dependence of (23) and (24) and arises after the appropriate digitization.

result in numbers of the same order from one height interval to the next. But even in this case we have to deal with another problem: Due to the weak wavelength dependence of the integrands in (23) and (24), the columns of $C_{ij\nu}$ and $D_{ij\nu}$ are almost linearly dependent as well.

Another problem, which still remains unsolved due to technical constraints is the number $\#\nu$ of the observed flux oscillations at different wavelengths. In order to find an exact solution of (25) we have to provide $2(N+L) = \#\nu$ equations. Since only seven different observations are available, it is possible to solve the inverse problem with $N = 2$ height points using the linear spline representation $L = 1$. This solution would not be satisfying in terms of the resolution along the height axis.

In order to overcome all the mentioned difficulties and especially to solve the problem for large numbers N, we abandoned the aim of finding the *exact* solution and tried finding a solution of (25) in the case if the total number of unknowns was higher than the number of the equations ($2(N+L) \gg \#\nu$). Such a case is called underdetermined and can be treated only with some extra restrictions. These are more or less arbitrary and always subjective. However, the aim is to find a solution that is less sensitive to the effects described above. One possibility is the minimum-norm solution (see Press et al. 2007). The norm of our solution vector x is given by $||x||^2 = x^T x$. The aim was to find the solution of (25) with the least norm.

The problem is commonly solved using the Lagrange multipliers λ:

$$J = 1/2||x||^2 + \lambda(\tilde{C}x - \delta F_\nu). \tag{26}$$

A minimization of the function J respective to the coordinates of x and λ leads to

$$x = \tilde{C}^T(\tilde{C}\tilde{C}^T)^{-1}\delta F_\nu, \tag{27}$$

where the matrix $\tilde{C}^T(\tilde{C}\tilde{C}^T)^{-1}$ is quadratic and is called pseudo inverse of the matrix $\tilde{C}$.

The described method has to be applied to real $A_\nu cos(\Delta\varphi_\nu)$ and imaginary $A_\nu \sin(\Delta\varphi_\nu)$ parts of the observed relative flux oscillations. This would provide solutions for amplitude and phase of δT and $\delta\rho$ separately.

6 Results

In this paper we have discussed the results obtained by means of adiabatic approximation and have shown the applicability of our method. The minimum-norm solutions of the inverse problem (25) will now be presented and different spline representations of $\delta T/T$ will be discussed. Our first results were obtained without integration over filters (12). We used them to show the general agreement between the solutions using linear, quadratic and cubic spline representations for different numbers of height points.

We are looking for complex solutions of the inverse problem

$$\delta T/T = \mathrm{Re}(\delta T/T) + \mathrm{i}\,\mathrm{Im}(\delta T/T) = |\delta T/T|\exp(\mathrm{i}\varphi), \tag{28}$$

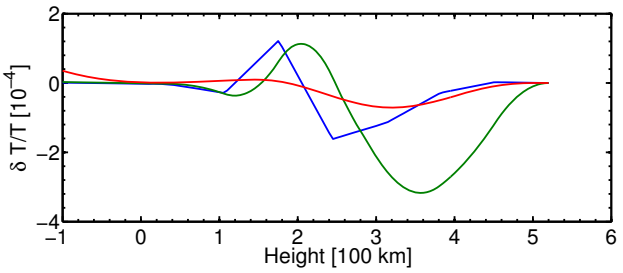

Fig. 11 Solutions of the inverse problem using polynomials of the first (blue), second (green), and third (red) order for $N = 10$ points.

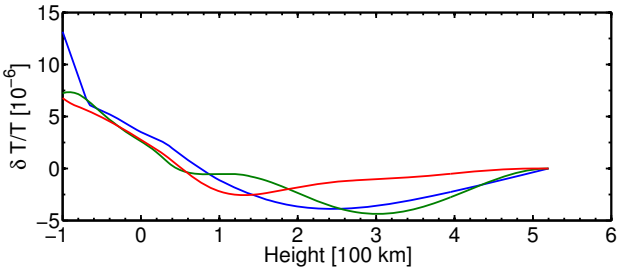

Fig. 12 Solutions of the inverse problem using polynomials of the first (blue), second (green), and third (red) order for $N = 20$ points.

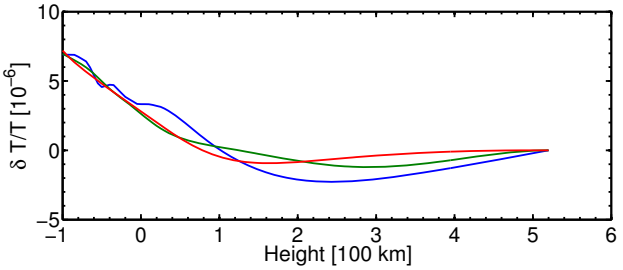

Fig. 13 Solutions of the inverse problem using polynomials of the first (blue), second (green), and third (red) order for $N = 40$ points.

which corresponds to the physical solution

$$|\delta T/T|\cos(\omega t + \varphi), \tag{29}$$

where $|\delta T/T|$ and φ are functions of depth. Figures 11–13 shows the solutions for different numbers of height points $N = 10, \ldots, 40$ (see Sect. 5) displaying solutions in form of $|\delta T/T|\cos\varphi$. This is a snapshot of one solution for a specific moment in time. It displays characteristic features of the solution. The plots of Figs. 11–13 show three different solutions for a specific number of points. These solutions are piecewise functions which consist of linear quadratic and cubic splines. In is not surprising that the solutions differ from each other because they refer to an ill-posed problem. The differences between solutions decrease with an increasing number of points. This suggests that solutions with a large number of points provide a better description of waves in the photosphere. Besides, solutions with 10 points (Fig. 11) show the large amplitudes of the temperature fluctuations $\delta T/T \approx 10^{-4}$. There are reasonable

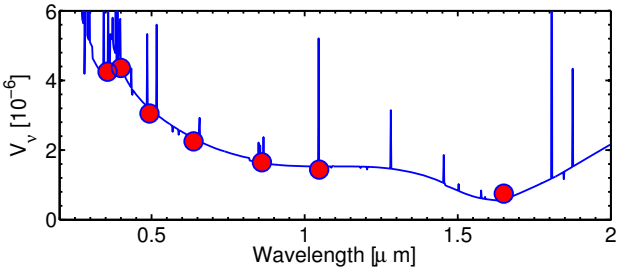

Fig. 14 Amplitude of the visibility function, calculated using the resulting δT. Red circles represent the observed amplitudes from Table 1.

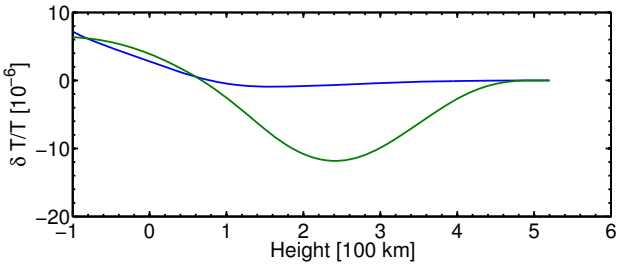

Fig. 15 Comparison of solutions with (green) and without (blue) considering the finite spatial resolution for linear spline and $N = 40$ height points.

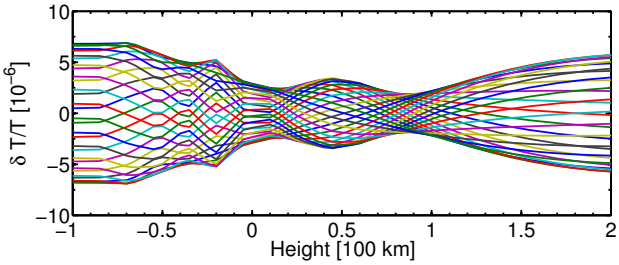

Fig. 16 Time-dependent linear spline solution for $N = 40$ height points using filters from Fig. 1.

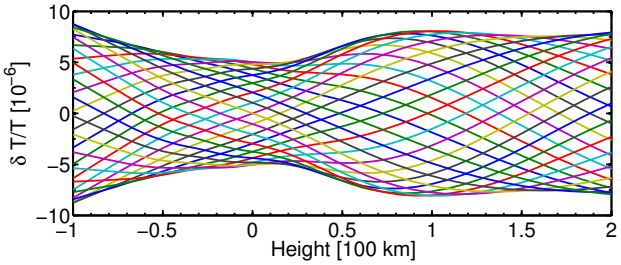

Fig. 17 Time-dependent quadratic spline solution for $N = 40$ height points using filters from Fig. 1.

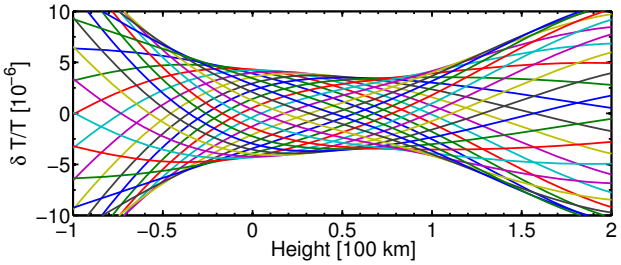

Fig. 18 Time-dependent cubic spline solution for $N = 40$ height points using filters from Fig. 1.

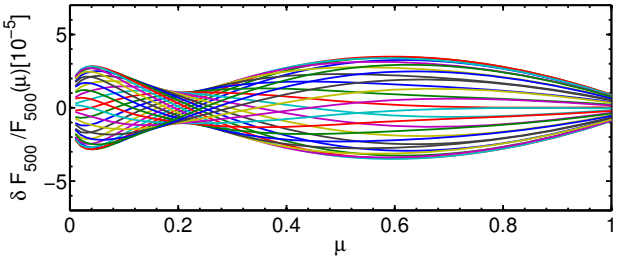

Fig. 19 Darkening function for $\delta F_\nu / F_\nu$ in time; linear spline.

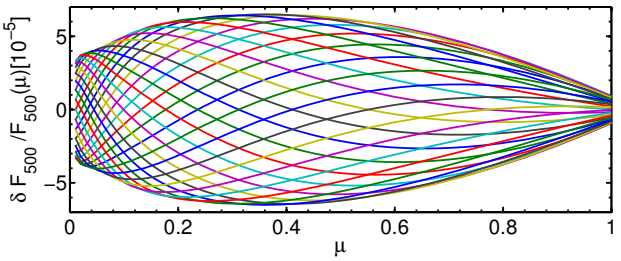

Fig. 20 Limb darkening function for $\delta F_\nu / F_\nu$ in time; quadratic spline.

doubts whether p-modes can produce similarly large temperature fluctuations in the photosphere. Relative fluctuations of temperature have to be of the same order as relative fluctuations of the solar flux, i.e. about 10^{-6}. The amplitude of temperature fluctuations in this case is about equivalent to the amplitude of temperature fluctuations of the Sun due to the solar cycle (Kopp & Lean 2011).

The remaining three sets (Figs. 12–13) for 20, 30, and 40 points show better agreements between solutions in deeper layers than in the top parts of the atmosphere. This is understandable because the contribution functions for all parts of the continuum as well as the difference between them decrease with height in photosphere. The accuracy of the solution of the inverse problem decreases with height due to this property of the contribution functions.

All solutions tend to zero at high altitudes – in contrast to the solution based on a single polynomial (Fig. 10). The reason for this behavior lies in the nature of our subjective choice of the form of the solution. On the one hand, we searched for a solution with the least possible norm, which is obviously zero. On the other hand, using the minimum norm method we had to satisfy the left hand side of Eq. (25), which is in general not zero. A compromise had to be found, which consists in satisfying Eq. (25) in the vicinity of $\tau_\nu = 1$ and allowing δT to reach zero in regions with $\tau_\nu \ll 1$, while affecting the left hand side of Eq. (25) as little as possible. However, we have to stress that all predictions considering the temperature behavior above 200 km ($\tau_\nu < 10^{-1}$), where significant differences between $\delta T/T$ occur, are pure speculations.

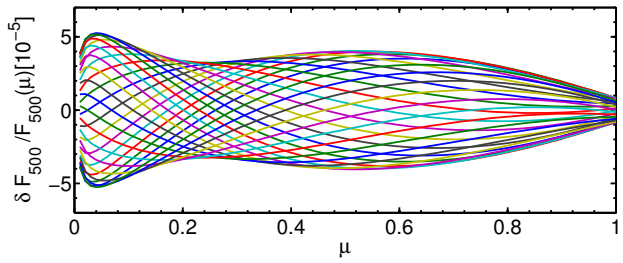

Fig. 21 Limb darkening function for $\delta F_\nu/F_\nu$ in time; cubic spline.

Using $\delta T/T$ from Figs. 11–13 we calculated $\delta F_\nu/F_\nu$ to check the observed values from Table 1. The relative errors are of the order of 10^{-8}–10^{-13}, depending on the choice of the spline (Fig. 14). Local thin peaks occur due to absorption lines and are not of interest. Of interest, however, is the increase in the visibility function near $2\,\mu$m, which is in contrast with Zhugzhda & Lebedev (2009), where a monotonic decreasing function was assumed.

Figures 11–13 show a convergence towards a steady solution. This fact is very important, since we are searching for a solution of an ill-posed problem. Thus we believe that the solution is also physically correct. However, we have to stress that this is only *one* of the possible solutions.

We explored the effect of averaging brightness fluctuations over the band defined by front-end filters of the photometers (Eqs. 12 and 13) on the solution of the inverse problem. Figure 15 shows that the averaging over filters affects the solutions. In particular, it increases the amplitudes of the temperature fluctuations. It is clear that the filters have to be taken into account.

In order to do a physical analysis of the solutions, the time behavior of the five-minute temperature disturbances was explored. Figures 16–18 show snapshots of the profile of five-minute temperature disturbances (Eq. 29) at different moments in time. The wave profiles at different moments are shown by different colors. The key question is whether p-modes have nodes and antinodes. All solutions show a standing wave at deep layers. The wavelength is about 100 kilometers. But there are not only standing waves, but also waves running through the photosphere, i.e. this is a combination of standing and running waves because the amplitude at nodes do not drop to zero.

7 Discussion

There are in principle two separate papers, dealing with the same problem. Stodilka (2005) solved the ill-posed inverse problem using the Tikhonov regularization and considered no finite spectral resolution of the DIFOS photometer. Rodríguez Hidalgo et al. (2001) obtained the solutions ($\rho(z)$, $T(z)$ and $v(z)$) of the inverse problem by means of Monte Carlo simulations for a local sector of the Sun. The results of both papers are comparable. Since there is no principal difference between local and global (observations of the sun as a star) oscillations, we will refer to the second paper and compare our results.

The analysis of the results faces difficulties due to shortcomings of the current theory of nonadiabatic waves. All explorations of nonadiabatic waves have been performed either for uniform media or for an isothermal atmosphere. The radiative flux through the atmosphere is entirely absent. The structure of the photosphere is, however, defined by the radiative flux which goes from deeper layers towards outer space. The p-modes produce fluctuations of opacity (kappa-effect) which result in fluctuations of the stellar brightness. This effect influences the properties of nonadiabatic waves. For example, in this case quasi-adiabatic waves have to differ from classical non-adiabatic waves. Classical nonadiabatic waves appear when the relaxation time exceeds considerably the period of oscillations. Relaxation times in the solar photosphere vary from tenth to hundreds of seconds, i.e. less or about one period of the five-minute oscillations. But the temperature relaxation due to blackbody radiation is partly compensated for by the kappa-effect. Consequently, five-minute quasi-adiabatic oscillations can occur in the solar photosphere. But the properties of this kind of oscillations were unfortunately not explored in the framework of simple models. Consequently, we do not know exactly whether the assumption (18) is correct in this case.

The classical theory of nonadiabatic waves (Zhugzhda 1983) predicts the coupling of nonadiabatic p-modes and radiation diffusion (temperature) waves. This coupling appears when $\omega t_{\rm R} \sim 1$. Consequently, the coupling of quasi-adiabatic waves is very weak. However, it is not clear whether the coupling between modes is absent in the case of quasi-adiabatic waves appearing due to a partial compensation of blackbody radiation by the kappa-effect. The linear solution (Fig. 16) displays a standing wave with a wavelength of about 100 km, similar to the results of Stodilka (2005) and Rodríguez Hidalgo et al. (2001). This wave can not be acoustic because its wavelength is too small: an acoustic 5-min wave would have a wavelength of about 6 Mm. The advantage of the Rodríguez Hidalgo et al. (2001) exploration is that it found the eigenfunction of local five-minute oscillations. This eigenfunction does not show any signs of the presence of standing waves. This is one more argument supporting the idea that radiation diffusion waves occur in the photosphere since this type of wave shows itself mostly in fluctuations of temperature and density and not in velocity. However, the wave signatures are less definite when quadratic and cubic splines are used. There has been evidence nodes move in the deeper layers. One possibility of checking the validity of our solutions is to look at the limb darkening functions of p-mode oscillations, which so far has not been done, neither by Stodilka (2005) nor by Rodríguez Hidalgo et al. (2001).

Figures 19–21 show the darkening functions at 493 nm for linear, quadratic, and cubic splines. In general, they agree with the predictions of Toutain & Gouttebroze (1993), especially our functions show a non-monotonic behavior

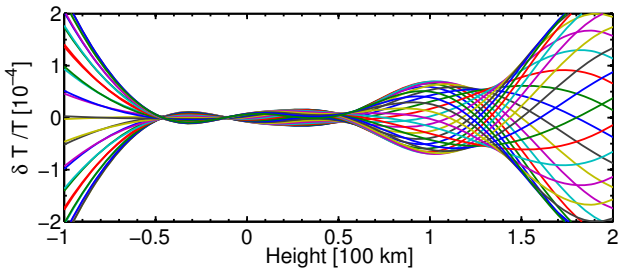

Fig. 22 The dependence of δT on depth if only blackbody radiation is taken into account.

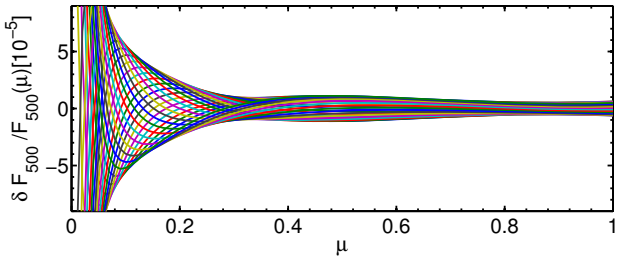

Fig. 23 The limb darkening function if only blackbody radiation is taken into account.

with decreasing μ. Any temperature perturbation would travel as a wave towards the limb, causing different flux oscillations. Our results were obtained without assuming that the temperature disturbances are proportional to their undisturbed values $\delta T/T \approx \mathrm{const}$, as was done by Zhugzhda et al. (1996).

It is important to stress that the solutions seem to be insensitive to the specific choice of the spline order, being therefore steady minimum-norm solutions of an ill-posed problem. However, the fact that they provide the observed visibilities means only that they have correct mean values. An additional comparison with Rodríguez Hidalgo et al. (2001) reveals general agreement also in shape, especially the existence of a broad (100–200 km) temperature minimum in the vicinity of $\tau_{500} = 1$. But only observations of the limb darkening functions can provide sufficient information to decide between the various solutions. Unfortunately, the limb darkening function of solar p-modes has not been explored so far.

One more experiment was done. The inverse problem was solved for the case when only black body radiation is responsible for the brightness oscillations of the Sun. Figures 22 and 23 show the eigenfunction of temperature disturbances and the limb darkening function for this case. There is an essential difference between this case and the case of a combined effect of blackbody radiation and kappa-effect. The solution shows short-wavelength waves. The wavelength of this waves is so short that their occurrence can be explained only by the appearance of radiation waves. We have already claimed that the kappa-effect has to be taken into account. An exploration of the limb darkening function is the best way to make a choice between the solutions.

8 Conclusions

The goal of this paper was to reconstruct the temperature fluctuations using the observational data from the DIFOS photometer, which resulted in an ill-posed problem. This problem was solved assuming a quasi-adiabatic approximation which is defined by condition (18). However, it is not clear whether this condition is valid in the case of quasi-adiabatic oscillations in the solar photosphere because these occur due to an approximate balance between blackbody radiation and kappa-effect. Besides, it is still an open question whether radiation diffusion waves appear in the solar photosphere due to coupling with nonadiabtic waves. This problem is important for the theory of brightness fluctuations of stars due to eigen-oscillations.

A few further steps are important for the exploration of the problem. First of all one needs to develop a method for the solution of the inverse problem for nonadiabatic waves without imposing the adiabatic condition. It is important to include more observational data in the analysis. The exploration of limb darkening functions is very important since the results of this exploration can be used or for the choice of the best solution or directly for the solution of the inverse problem.

Our view on the importance of the kappa-effect differs from the conclusions of Toutain & Gouttebroze (1993). This difference can be associated with the fact that their exploration was done at a time when data of SoHO and CORONAS were not yet available. There is an important difference between the analysis of observational data by Toutain & Gouttebroze (1993) and the current paper: We take into account not only the amplitudes of brightness for different ranges of wavelength but also phase shifts between these amplitudes. This changes the results considerably.

Acknowledgements. We thank H. Uitenbroek for providing us with the newest version of his code. Y.D. is thankful to DFG for support in frames MERCATOR program. We also thank Judith Blank for reading our paper and correcting the language.

References

Ballot, J., Barban, C. & van't Veer-Menneret. C. 2011, A&A, 531, A124
Fontenla, J. M., Avrett, E., Thuillier, G., & Harder, J. 2006, ApJ, 639, 441
Hasler, K.-H., Zhugzhda, Y. D., Lebedev, N. I., Arlt, R., & Oraevsky, V. N. 1997, A&A, 322, L41
Kopp, G. & Lean, J. L. 2011, Geophysics Research Letters, 38, L01706
Kunasz, P. & Auer, L. H. 1988, JQRST, 39, 67
Kurucz, R. L. 1969, ApJ, 156, 235
Lebedev, N. I., Oraevsky, V. N., Zhugzhda, Y. D., et al. 1995, A&A, 296, L25
Mihalas, D. 1970, Stellar Atmospheres (W. H. Freeman and Co.)
Mihalas, D., Mihalas, B. W. 1984, Foundations of Radiative Hydrodynamics (Oxford University Press)
Nutto, C., Roth, M., Zhugzhda, Y., Bruls, J., & von der Lühe, O. 2008, Sol. Phys., 251, 179

Press, W. H., Teukolsky, S. A., & Vetterling, W. T. 2007, Numerical Recipes (Cambridge University Press)
Rodríguez Hidalgo, I., Ruiz Cobo, B., Collados, M., & Bellot Rubio, L. R. 2001, ApJ, 547, 491
Rybicki, G. B. & Hummer, D. G. 1992, A&A, 262, 209
Staude, J., Dzhalilov, N. S., & Zhugzhda, Y. D. 1994, Sol. Phys., 152, 227
Stodilka, M. I. 2005, Kosmichna Nauka i Tekhnologiya, 11, 010000
Toutain, T. & Gouttebroze, P. 1993, A&A, 268, 309
Uitenbroek, H. 2001, ApJ, 557, 389
Wehrli, C., Fröhlich, C., Anklin, M., et al. 1997, in Correlated Phenomena at the Sun, in the Heliosphere and in Geospace, ed. A. Wilson, ESA Special Publication, Vol. 415, 497
Zhugzhda, I. D. 1983, APSS, 95, 255
Zhugzhda, Y. D., Dzhalilov, N. S., & Staude, J. 1993, A&A, 278, L9
Zhugzhda, Y. D. & Lebedev, N. I. 2009, Astronomy Letters, 35, 494
Zhugzhda, Y. D., Staude, J., & Bartling, G. 1996, A&A, 305, L33+

